Active Disturbance Rejection Control Strategy for Grid-Connected Photovoltaic Inverter Based on Virtual Synchronous Generator

YUNJUN YU[ID], (Member, IEEE), AND XIANGYU HU
School of Information Engineering, Nanchang University, Nanchang 330031, China

Corresponding author: Yunjun Yu (yuyunjun@ncu.edu.cn)

ABSTRACT In order to solve the problem of insufficient control performance of various traditional control strategies in the complex environment of grid-connected inverters, the active disturbance rejection control (ADRC) strategy based on the virtual synchronous generator (VSG) is proposed. The mathematical model of a grid-connected photovoltaic inverter based on the VSG is built. The proposed control strategy provides the inverter with more disturbance attenuation and provides rotational inertia. The control strategy estimates and compensates the total disturbance and generates the reference active power and reactive power by ADRC. The control strategy converts the three-phase voltage and current outputs into positive and negative sequences on the *dq* reference frame. The VSG control module generates a reference voltage command and outputs it to the dual closed loop PI feedforward decoupling control. The PWM signal is finally obtained by the PI feedforward decoupling control. The ADRC strategy based on the VSG does not change the original control characteristics of the VSG; it retains the characteristics of the synchronous generator, and it also provides inertia and damping for the power grid. The simulation shows that the ADRC strategy based on the VSG applied to the inverter can attenuate disturbances. Under the unfavorable conditions of the unstable reference power, such as the unbalanced three-phase voltage and the random disturbance, the output power matches the international electricity standard.

INDEX TERMS Virtual synchronous generator (VSG), active disturbance rejection control (ADRC), power control, grid-connected inverter, positive and negative separation.

I. INTRODUCTION

With the increasing number of renewable power generations which including a lot of power electronics devices that do not provide inertia in the power grid system, the proportion of synchronous generators that provide system inertia is decreased, which results in a decrease in the total inertia of the system. When the load power changes, for example, it increases by 50\%, the power grid frequency does not match the IEC standard, which will have an adverse effect on the stable operation of the power grid and the generator [1]. Because of the slow response of PID control, dynamic disturbances cannot be quickly attenuated or unattenuated, the controller performance become worse. The linear weighting

of proportional, integral and derivative links does not reach the optimal control and they are not the optimal combination [2]. The output power can be tracked by PQ control. However, the control accuracy is bad, the disturbance cannot be attenuated by PQ control in the case of a significantly disturbance. This makes the reference power cannot be well tracked. Droop control simulates the drooping characteristics of the synchronous generator. The inverter feeds back the detected active power and reactive power back to input, and multiplies the command value of the output voltage amplitude and voltage frequency by a droop coefficient. It obtains the system voltage amplitude and power angle which meet the requirements of the power grid [3]. Droop control structure is simple and its performance is reliable, But the output of droop control is not satisfied, the inertia for the system cannot be provided, when the load

power changes, the fluctuation of the grid frequency cannot be attenuated [4]. In [5], an ADP algorithm for suppressing random disturbances is proposed, which uses reinforcement learning and adaptive dynamic programming to obtain an optimal controller. However, the combination of ADP and other algorithms, the stability and convergence of the controller cannot be guaranteed. The ideal grid-connected photovoltaic inverter can not only provide high-quality power to the power grid, but also can support the frequency and voltage amplitude of the power grid. In case of unknown disturbance, the disturbance can be attenuated as much as possible to ensure that the power grid is safe and stable. In conventional power systems, a large number of synchronous generators provide sufficient system rotational inertia to support the grid voltage and grid frequency. However, the physical structure of distributed inverters and synchronous generators are so different that distributed inverters cannot provide inertia [6].

A VSG-based ADRC method was proposed, which added an ADRC module in addition to the original VSG controller. It is used to solve the stability problem of the grid-connected inverter, and ensure the synchronization of the grid-connected inverter when the grid-connected inverter is disturbed. The VSG simulates the behavior of the synchronous generator and simulates the oscillation equation of the synchronous generator to express the virtual inertia [7]. Similar to the droop control, the VSG controller simulates the characteristics of the generator. The reference active power and reactive power as the input to the VSG controller, the voltage amplitude and phase angle are obtained by the VSG controller. However, VSG control provides virtual inertia to the system and has better control accuracy than droop control. [8]. VSG is divided into voltage type and current type. The current type VSG control strategy is suitable for low-permeability power grid environment, and voltage type VSG is suitable for high-permeability power grid environment [9]. This paper uses a voltage type VSG control strategy. The VSG can provide the system with the features of frequency regulation and voltage regulation. In [10], VSG is used to control the output frequency and power. However, the addition of the VSG also brings oscillation risks, especially in complex environment. VSG control will have dynamic instability under significantly disturbances, the dynamic stability of the system will be affected by the significantly disturbance. In [11], the stability problem of synchronous motor under small disturbance is analyzed. In [12], the power control of the VSG when the grid frequency change and the grid voltage change is proposed, the control strategy can output constant active power and constant reactive power. When the grid voltage is unbalanced, the proposed control strategy will fail. In [13], a VSG control strategy is proposed, in the case of voltage dips to enhance the VSG's low-voltage ride-through capability so that the inverter would not be off-grid in the event of a voltage dip. In order to ensure that the inverter can work in a complex environment and solve the stability problem of VSG control to further reduce the steady-state error, the ADRC module is added. The ADRC combines the advantages of PID

control but overcomes the disadvantages of slow response and easy overshoot in PID control [14]. The ADRC does not depend on the exact model of the controlled system. It only needs to know the order and approximate gain of the controlled system, then an ADRC can be designed [15]. In [2] and [16]–[19], ADRC is used in different control systems and has good control performance. In [20] and [21], ADRC is combined with other control methods and has good control performance. In [22], An improved ADRC was proposed and used in nonlinear systems. There are mainly three parts of the ADRC, which is the tracking differential(TD), linear state error feedback law(LSEF), and extended state observer(ESO) [23]. ADRC is a similar control strategy to the improved PID control with better control performance [24]. ADRC can effectively attenuated unknown disturbances and has excellent adaptability to external disturbances, which can guarantee the closed-loop stability of the system [25], [26].

In this paper, an ADRC strategy based on a VSG is proposed. the outer loop is ADRC, the inner loop is VSG. The mathematical model of the inverter and the mathematical model of the controller is analyzed in detail in section II. In section III, some compensation is added to the final output of the controller, which enhances the ability to attenuate disturbances. In section IV, simulations are carried out in different situations, and the proposed strategy is realized.
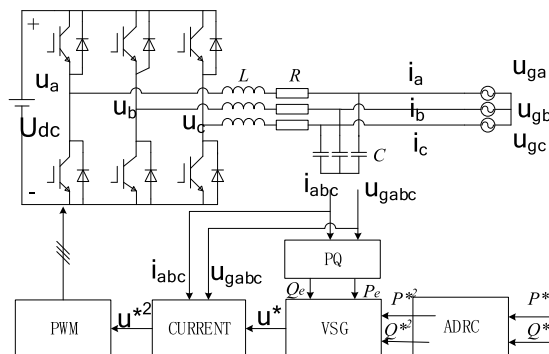

FIGURE 1. ADRC block diagram based on VSG.

II. ADRC STRATEGY BASED ON VSG

A block diagram of ADRC based on VSG is showed in Figure 1. VSG control is a control strategy that simulates the working principle of synchronous generator. It makes the inverter have the external characteristics of synchronous generator and provides inertia for the system. However, the effect of individual VSG control is not ideal. In the case of external disturbances, the disturbance of the output power cannot be suppressed. ADRC is a new type of controller that retains the basic framework of PID control but improves local functions. It can suppress disturbances very well. In Figure 1, U_{dc} is the DC side voltage source, R is the equivalent line resistance, L is the inductance, C is the filter capacitor, i_a, i_b, i_c are the output three-phase current of the inverter side respectively, Assume that the filter capacitor is ignored, which is means the three-phase current on the inverter side is the same as

the three-phase current on the grid side. u_a, u_b, u_c are the output three-phase voltage on the inverter side. u_{ga}, u_{gb}, u_{gc} are the three-phase voltage on the grid side. P* and Q* are the active power and reactive power, which are calculated by u_{gabc}, i_{abc}. P* and Q* are the reference values of active power and reactive power. As shown in Figure 1, P* and Q* use an ADRC algorithm to output P^{*1} and Q^{*1}, P^{*1} and Q^{*1} contain disturbance information. We can obtain the amplitude and phase angle of the inverter output voltage through the VSG control, and output the three-phase voltage, next, through the current calculation and the current decoupling control loop, Transform the three-phase voltage into obtain the three-phase modulation signal output to the PWM to control the IGBT. Under this control strategy, the reference power can be well tracked by the power output by the inverter.

A. INVERTER MODELING

Consider the inverter in Figure 1, ignoring the effect of the filter capacitor, it can establish the relationship between the voltage on the inverter side, the voltage of the grid, and the inverter output current.

$$R i_{abc} + L \frac{d i_{abc}}{dt} = u_{abc} - u_{gabc} \quad (1)$$

In Equation 1, u_{abc}, i_{abc}, u_{gabc} are the inverter side voltage, side current and grid voltage, L is the inductance and R is line resistance. Grid-connected inverter output active power and reactive power are:

$$\begin{cases} P = u_{ga}i_a + u_{gb}i_b + u_{gc}i_c \\ Q = (u_{ga}i_a + u_{gb}i_b + u_{gc}i_c)/\sqrt{3} \\ S = e_{g\alpha\beta}\hat{i}_{\alpha\beta} \end{cases} \quad (2)$$

B. VSG CONTROL STRATEGY

The principle of a synchronous generator is simulated by VSG. The VSG control consists of two links, active power control and reactive power control [27]. In VSG the active power control is used to adjust the frequency, corresponds to the speed control system and introduces the inertia and damping links in the active power control. The reactive power is used to adjust the voltage amplitude, corresponding to the excitation system, making the external characteristics of the inverter and the traditional Synchronous generator are similar, which can provide the rotational inertia to ensure the smooth operation of the grid. According to the structure of a synchronous generator, the VSG control links are designed [28].

As shown in Figure 2, J and K are the integral coefficients, D is the damping coefficient, w_g is the rated angular velocity, U and *P* are the output voltage amplitude and phase angle respectively, and u_{abc} is the three-phase Voltage. The P-f control of the VSG realizes the control of the output phase angle *P* at the inverter side by subtracting the given active power from the actual active power. The Q-V control link realizes the voltage tracking by subtracting the given reactive power and the actual reactive power. The inverter side voltage
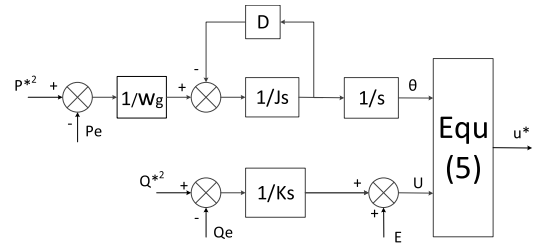

FIGURE 2. VSG control block diagram.

amplitude U is controlled by U and *P* to generate the inverter command voltage u_{abc} [29].

Active power control:

$$\begin{cases} \dfrac{dw}{dt} = \dfrac{1}{J}\left\{ \dfrac{1}{w_0}\left(P^{*2} - P_e\right) - w \right\} \\ \dfrac{dw}{dt} = (w + w_g + w_0) \end{cases} \quad (3)$$

Reactive power control:

$$\frac{dU}{dt} = K(Q^{*2} - Q) \quad (4)$$

$$u^* = \begin{bmatrix} U\sin(\theta) \\ U\sin(\theta - 2\pi/3) \\ U\sin(\theta + 2\pi/3) \end{bmatrix} \quad (5)$$

C. CURRENT COMMAND CONTROL

According to the mathematical model of the inverter, the current command calculation equation and the PI decoupled current control loop can be obtained. The ratio of inductance and resistance in the low-voltage line of the micro-grid is small, there is a coupling between the active and reactive power controlled by the VSG, and the dominant virtual reactance can be introduced in the control section of the inverter. In other words, a virtual impedance control link is added, dq-axis current command is generated. Then, through the feed forward PI decoupling control, the dq-axis modulation voltage is generated, and the three-phase modulation voltage is converted to the abc reference frame is output to the PWM.

Ignoring the effect of the inverter filter capacitor, the relationship between and the inverter side current and the voltage and the grid voltage can be obtained. This is a simple mathematical model of the inverter. We can take the synchronous generator equation and the inverter mathematical equation as the prototype, and then the relationship between VSG output voltage and command current and grid voltage are obtained. i_{abc}, u_{gabc}, u_{abc}^* are current command values, grid voltage, and VSG output voltage in the abc reference frame.

$$R \begin{bmatrix} i_d^* \\ i_q^* \end{bmatrix} + X \begin{bmatrix} -i_q^* \\ i_d^* \end{bmatrix} = \begin{bmatrix} u_d^* \\ u_q^* \end{bmatrix} - \begin{bmatrix} u_{gd} \\ u_{gq} \end{bmatrix} \quad (6)$$

$$\begin{bmatrix} R & -X \\ X & R \end{bmatrix} \begin{bmatrix} i_d^* \\ i_q^* \end{bmatrix} = \begin{bmatrix} u_d^* \\ u_q^* \end{bmatrix} - \begin{bmatrix} u_{gd} \\ u_{gq} \end{bmatrix} \quad (7)$$

$$\begin{bmatrix} i_d^* \\ i_q^* \end{bmatrix} = \frac{1}{R^2 + X^2} \begin{bmatrix} R & X \\ -X & R \end{bmatrix}$$

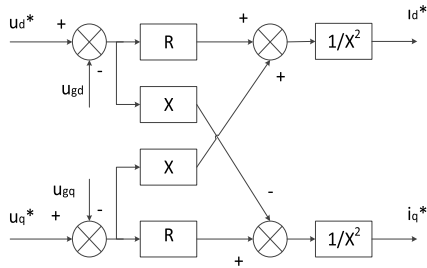$$\times \left(\begin{bmatrix} u_d^* \\ u_q^* \end{bmatrix} - \begin{bmatrix} u_{gd} \\ u_{gq} \end{bmatrix} \right) \quad (8)$$

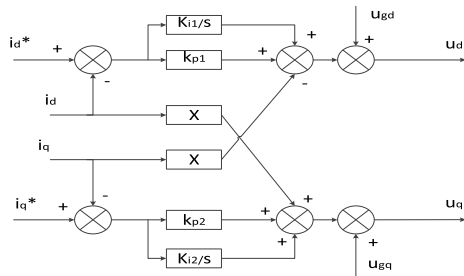**FIGURE 3.** Virtual impedance control block diagram.

FIGURE 4. PI decoupling control block diagram.

In equation 8, u_d^* and u_q^* are the dq-axis voltage components obtained by the dq transformation of the reference voltage; u_{gd} and u_{gq} are the dq-axis components of the grid voltage; i_d^* and i_q^* are the current command values, and they are the output of the virtual impedance control link, which output the three-phase modulation voltage through the feedforward decoupling control link. Feed forward decoupled PI control is shown below.

$$\begin{cases} \dfrac{du_{d1}}{dt} = k_{i1}\left(i_d^* - i_d\right) \\ \dfrac{du_{q1}}{dt} = k_{i2}\left(i_q^* - i_q\right) \\ u_d = u_{d1} + k_{p1}\left(i_d^* - i_d\right) - Xi_q + u_{gd} \\ u_q = u_{q1} + k_{p2}\left(i_q^* - i_q\right) + Xi_d + u_{gq} \end{cases} \quad (9)$$

D. ADRC STRATEGY

There are three main parts of the ADRC, TD, LSEF, and ESO. The TD is a transition link, makes the given signal filtered, filters out possible interference at the input, and the phase is corrected [30]. The LSEF adds the given signal which is processed by the TD and the signal which is feedback by the ESO together, plus the total disturbance, it can be seen as the control signal of the controlled target [31]. For an inverter with LC filtering, ignoring the role of the capacitor, it can be seen as a first-order controlled object, a first-order ADRC is designed for it, and the (ESO) is second-order for ease of control and parameter tuning. The linear observer is selected for the (ESO) and the ADRC is designed is as follows. In the same way, the same ADRC is designed for reactive power.

First-order TD:

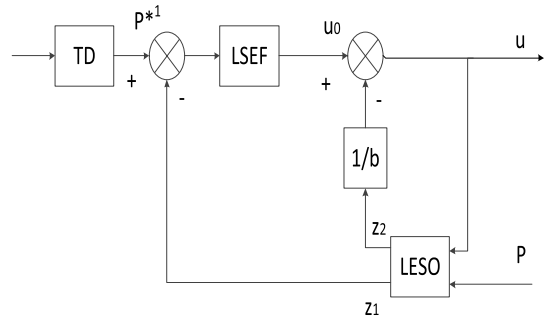$$\begin{cases} e_1 = P^{*1} - P^* \\ \dot{P}^{*1} = -re_1 \end{cases} \quad (10)$$

FIGURE 5. First-order ADRC block diagram.

linear ESO:

$$\begin{cases} e_2 = z_1 - p \\ \dot{z}_1 = z_2 - \beta_1 e_2 + bu \\ \dot{z}_2 = -\beta_2 e_2 \end{cases} \quad (11)$$

First-order LSEF:

$$\begin{cases} e_3 = P^{*1} - z_1 \\ u_0 = ke_3 \\ u = u_0 - z_1/b \end{cases} \quad (12)$$

For the ADRC, there are four parameters that need to be coordinated and set. They are $k\beta_1$, β_2, b. β_2 and b affect the observer's estimated output of disturbance and improve the response speed of the system. β_1 inhibits overshoot and oscillation [32]. The poles of the ESO are configured and then the characteristic equation of the ESO can be obtained

$$D(S) = s^2 + \beta_1 s + \beta_2.$$

The stability condition is that the roots of D(S) is located in the left half of the s plane. $\beta_1 > 0$ and $\beta_2 > 0$ can guarantee controller stability [33]. In order to enhance the stability margin of the system, the root of the characteristic equation is kept away from the imaginary axis. When the roots of the characteristic equations are the same, the system is the most stable, there is $\beta_1^2 = 4\beta_2$. The bandwidth w_0 of the ESO is introduced, and the pole of the observer is arranged at $-w_0$. There is $\beta_1 = 2w_0$, $\beta_2 = w_0^2$. In actual parameter adjustment, it is not necessary to strictly adjust in accordance with this rule. By selecting appropriate parameters, we can make the control performance meet the requirements.

III. ANALYSIS OF ADRC DESIGN BASED ON VSG
A. IMPROVEMENT OF VSG CONTROL STRATEGY
When the inverter is connected to the grid, the active and reactive power of the inverter output is required to track the reference value [34]. However, when the three-phase voltage of the power grid is unbalanced, the output voltage of the inverter is controlled by the power grid, and the output voltage is three-phase unbalanced, and the power fluctuation is suppressed as a control target. Considering the unbalanced power grid, the output power of the grid-connected inverter can be derived from the following equations.

The mathematical model of grid voltage

$$\begin{bmatrix} u_{ga} \\ u_{gb} \\ u_{gc} \end{bmatrix} = \begin{bmatrix} E^+ cos\,(w_0t + \theta) \\ E^+ cos\,(w_0t + \theta - 120°) \\ E^+ cos\,(w_0t + \theta + 120°) \end{bmatrix}$$
$$+ \begin{bmatrix} E^- cos\,(w_0t + \theta) \\ E^- cos\,(w_0t + \theta + 120°) \\ E^- cos\,(w_0t + \theta - 120°) \end{bmatrix} \quad (13)$$

In the $\alpha\beta$ axis:

$$\begin{bmatrix} u_{g\alpha} \\ u_{g\beta} \end{bmatrix} = \begin{bmatrix} u_{\alpha}^+ \\ u_{\beta}^+ \end{bmatrix} + \begin{bmatrix} u_{\alpha}^- \\ u_{\beta}^- \end{bmatrix}$$
$$= \begin{bmatrix} E^+ cos\,(w_0t + \theta) \\ E^+ sin\,(w_0t + \theta) \end{bmatrix} + \begin{bmatrix} E^- cos\,(w_0t + \theta) \\ -E^- sin\,(w_0t + \theta) \end{bmatrix} \quad (14)$$

Equation 14 is represented as a vector

$$u_{g\alpha\beta} = E^+ e^{j(w_0t + \theta)} + E^- e^{-j(w_0t + \theta)} \quad (15)$$

Expressed on the dq axis

$$u_{g\alpha\beta} = u_{gdq}^+ e^{j(w_0t + \theta)} + u_{gdq}^- e^{-j(w_0t + \theta)} \quad (16)$$

The mathematical model of current:

$$\begin{bmatrix} i_{\alpha} \\ i_{\beta} \end{bmatrix} = \begin{bmatrix} i_{\alpha}^+ \\ i_{\beta}^+ \end{bmatrix} + \begin{bmatrix} i_{\alpha}^- \\ i_{\beta}^- \end{bmatrix}$$
$$= \begin{bmatrix} I^+ cos\,(w_0t + \theta) \\ I^+ sin\,(w_0t + \theta) \end{bmatrix} + \begin{bmatrix} I^- cos\,(w_0t + \theta) \\ -I^- sin\,(w_0t + \theta) \end{bmatrix} \quad (17)$$
$$i_{\alpha\beta} = I^+ e^{j(w_0t + \theta)} + I^- e^{-j(w_0t + \theta)} \quad (18)$$
$$i_{\alpha\beta} = i_{dq}^+ e^{j(w_0t + \theta)} + i_{dq}^- e^{-j(w_0t + \theta)} \quad (19)$$

Output Power:

$$S = u_{\alpha\beta} \hat{i}_{\alpha\beta} = \left(e_{dq}^+ e^{j(w_0t + \theta)} + e_{dq}^- e^{-j(w_0t + \theta)} \right)$$
$$\times \left(i_{dq}^+ e^{-j(w_0t + \theta)} + i_{dq}^- e^{j(w_0t + \theta)} \right) \quad (20)$$

$$P = P^0 + P_{cos} cos2\,(w_0t + \theta) + P_{sin} sin2\,(w_0t + \theta) \quad (21)$$

$$\begin{cases} P^0 = u_{gd}^+ i_d^+ + u_{gq}^+ i_q^+ + u_{gd}^- i_d^- + u_{gq}^- i_q^- \\ P_{cos} = u_{gd}^- i_d^+ + u_{gq}^- i_q^+ + u_{gd}^+ i_d^- + u_{gq}^+ i_q^- \\ P_{sin} = u_{gq}^- i_d^+ - u_{gd}^- i_q^+ - u_{gq}^+ i_d^- + u_{gd}^+ i_q^- \end{cases} \quad (22)$$

$$Q = Q^0 + Q_{cos} cos2\,(w_0t + \theta) + Q_{sin} sin2\,(w_0t + \theta) \quad (23)$$

$$\begin{cases} Q^0 = u_{gq}^+ i_d^+ - u_{gd}^+ i_q^+ + u_{gq}^- i_d^- - u_{gd}^- i_q^- \\ Q_{cos} = u_{gq}^- i_d^+ - u_{gd}^- i_q^+ + u_{gq}^+ i_d^- - u_{gd}^+ i_q^- \\ Q_{sin} = -u_{gd}^- i_d^+ - u_{gq}^- i_q^+ + u_{gd}^+ i_d^- + u_{gq}^+ i_q^- \end{cases} \quad (24)$$

Therefore, we have obtained the active power and reactive power of the inverter output under the grid voltage imbalance. In the above equation, P^0 and Q^0 are the average values of the output active power and reactive power respectively, P_{cos}, P_{sin}, Q_{cos}, Q_{sin} are output active power and reactive power fluctuation amplitudes, respectively. In order to suppress the fluctuation of the active power, the output active power should not contain a fluctuating component. We can make $P_{cos} = P_{sin} = 0$, positive and negative sequence current command values can be compensated, The original

control structure is unchanged, Positive sequence and negative sequence instructions are separately controlled. The compensated positive and negative sequence current command values are:

$$\begin{cases} i_d^{*+} = i_d^* \left(1 - k_{dd}^2 - k_{qd}^2 \right) \\ i_q^{*+} = i_q^* \left(1 + k_{dd}^2 + k_{qd}^2 \right) \\ i_d^{*-} = -i_d^- + \left(-k_{dd} i_d^* - k_{qd} i_q^* \right) \\ i_q^{*-} = -i_q^- + \left(k_{dd} i_q^* - k_{qd} i_d^* \right) \end{cases} \quad (25)$$

In equation 25, $k_{dd} = e_d^-/e_d^+, k_{qd} = e_q^-/e_d^+$. In order to suppress the fluctuation of the reactive power, that is mean the output active power does not contain a fluctuating component, $P_{cos} = P_{sin} = 0$, Positive and negative sequence current command values can be compensated.

$$\begin{cases} i_d^{*+} = i_d^* \left(1 + k_{dd}^2 + k_{qd}^2 \right) \\ i_q^{*+} = i_q^* \left(1 - k_{dd}^2 - k_{qd}^2 \right) \\ i_d^{*-} = -i_d^- + \left(k_{dd} i_d^* + k_{qd} i_q^* \right) \\ i_q^{*-} = -i_q^- + \left(-k_{dd} i_q^* + k_{qd} i_d^* \right) \end{cases} \quad (26)$$

B. CONTROLLER PARAMETER ADJUSTMENT

The VSG can simulate the characteristics of a synchronous generator. When the ADRC is not added, the parameters of the VSG are adjusted. When the stability of the VSG is satisfied, the values of the moment of inertia and the damping coefficient are reasonably adjusted to make the VSG have moderate damping and short response time. ADRC has four parameters that need to be set. They are β_1, β_2, b, k. Use pole placement method and bandwidth method to simplify the number of parameters, get a set of suitable parameters, and then slightly change the values of β_1 and β_2, so that ADRC has a stronger ability to suppress disturbances and improve response speed.

IV. SIMULATION

The ADRC strategy of the grid-connected three-phase inverter based on the VSG is simulated in the MATLAB.

The voltage on the DC side of the three-phase grid-connected inverter is 1000V, the resistance on the filter inductor is 0.001Ω, the inductance is 0.005H, and the filter capacitance is 0.000001F. In the VSG module, the damping coefficient D is 1, the rotor inertia J is 0.005, and the reactive power control integral coefficient K is 1. In the ADRC module, $\beta_1 = 95$ $\beta_2 = 3800$ b $= 1900$ k $= 200$. Then, set the reference value of active power equal to 5000W, and set the reference value of reactive power equal to 3000W. For the two cases of grid voltage three-phase unbalance and reference power abrupt change, the VSG-based ADRC strategy proposed which is compared with VSG control strategy. By contrast, the effectiveness of the VSG-based ADRC strategy in this paper is verified.

A. ACTIVE POWER CONTROL UNDER VOLTAGE IMBALANCE

The output active power of each control strategy under three-phase voltage imbalance are showed in Figure 7. As shown in Figure 6, phase A suddenly drops at 1s, is reduced to half the original voltage. The three-phase voltage is unbalanced, VUF$= |\frac{\vec{V_2}}{\vec{V_1}}| = 20\%$.
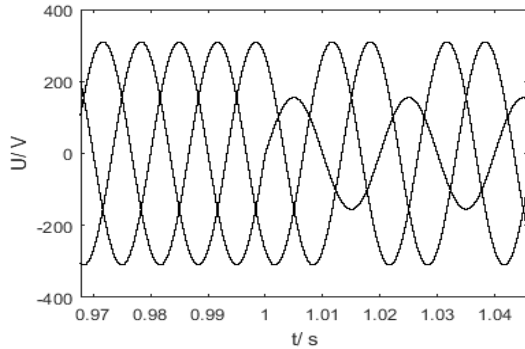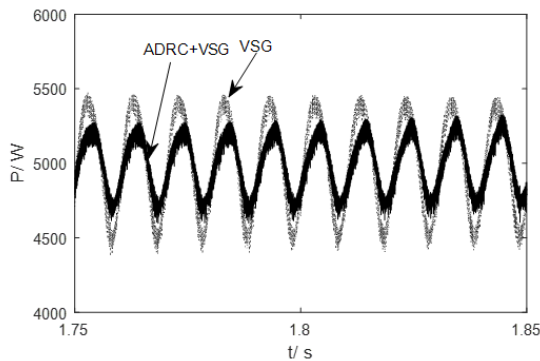

FIGURE 6. Three-phase voltage imbalance.

FIGURE 7. Comparison of two control strategies for three-phase unbalance.

The output active power comparison of the two control strategies under three-phase unbalance are showed in Figure 7. At 1 s, the three-phase voltage of the grid is unbalanced. It can be clearly seen from the figure that under the VSG-based ADRC strategy, the output active power has a maximum amplitude of 5300W and a minimum amplitude of 4600W. Under the VSG control strategy, the maximum output power is 5500W and the minimum amplitude is 4400W. The VSG-based ADRC strategy has the lowest power fluctuation amplitude. Compared with the VSG control strategy, the power fluctuation amplitude is reduced by 36.3%.

B. ACTIVE POWER CHANGE

Simulation result of the inverter output power when the reference power changes are showed in Figure 8. From 0 to 1 second, the reference active power is 5000W. At 1s, the load of the power grid increases, the required active power increases to 6000W, Increase the output power of photovoltaic array by 20%, and the reference active power jumps
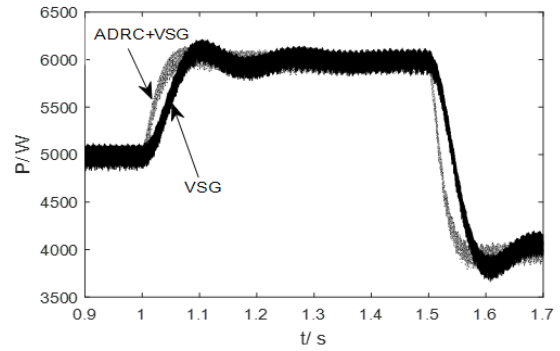

FIGURE 8. Comparison of two control strategies under power abrupt change.
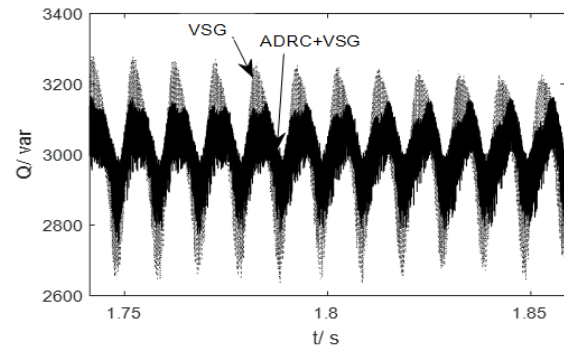

FIGURE 9. Comparison of two control strategies under voltage imbalance.

to 6000W. the load of the power grid is reduced, the required active power is reduced to 4000 W, the output power of the PV array is reduced by 20%. Compared to the original output power. and the reference active power is abruptly changed to 4000 W.

Comparison of the two control strategies in the case of a sudden change in active power are showed in Figure 8. that the VSG-based ADRC is in contrast to the VSG control, and the active power under the VSG-based ADRC strategy reaches the reference value faster, and the power does not fluctuate significantly.

C. REACTIVE POWER CONTROL UNDER VOLTAGE IMBALANCE

The output reactive power of each control strategy under three-phase voltage imbalance are showed in Figure 9. Phase A drops at 1s, it is reduced to half the original voltage. The three-phase voltage unbalance VUF$= |\frac{\vec{V_2}}{\vec{V_1}}| = 20\%$.

Output reactive power comparison of the TWO control strategies under three-phase unbalance are showed in Figure 9. At 1 s, the three-phase voltage of the grid is unbalanced. It can be clearly seen from the figure, under the VSG-based ADRC strategy, the output reactive power has a maximum amplitude of 3150var and a minimum amplitude of 2800var. Under the VSG control strategy, the maximum output power is 3300var and the minimum amplitude is 2650var. The VSG-based ADRC strategy outputs the lowest power fluctuation amplitude. Compared with the VSG

control strategy, the power fluctuation amplitude is reduced by 46.2%.

D. REACTIVE POWER CHANGE

Simulation result of the inverter output power with reference to the reactive power abrupt change are showed in Figure 10. From 0 to 1 second, the reference reactive power is 3000var. at 1s, the reference reactive power is increased to 4000var, and the reference reactive power is reduced to 2500var at 1.5s.
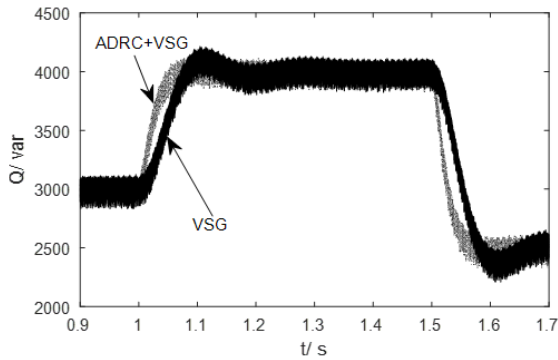

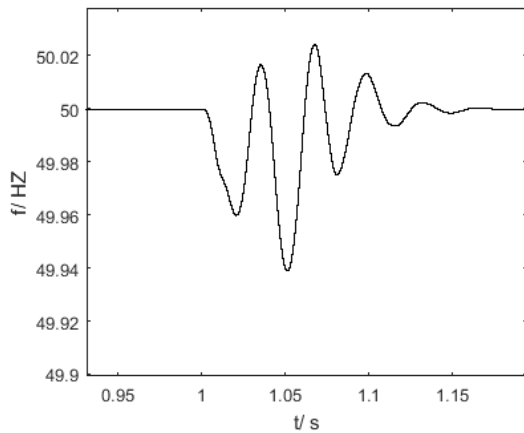**FIGURE 10.** Comparison of two control strategies under power abrupt change.

FIGURE 11. Frequency variation under voltage imbalance.

Comparison of two control strategies in the case of a big change in reactive power are showed in Figure 10. the VSG-based ADRC is compared with the VSG control, and the reactive power under the VSG-based ADRC reaches the changed reference value faster. Figure 11 shows the frequency variation of the control strategy in the case of sudden voltage imbalance, showing the support characteristics of the proposed control strategy for frequency.

E. OUTPUT POWER IN THE CASE OF DISTURBANCE

In order to verify the suppression effect of the control strategy on the continuous random disturbance, a white noise is added to the current output from the inverter as the disturbance source, the noise power is 0.1W, and the sampling time is0.01s. Compare VSG-based ADRC strategy with VSG control strategy, the simulation diagram of output active

power and reactive power are obtained. The magnitude of the power oscillation can be expressed by the root mean square error(RMSE) of the output power, $RMES = \sqrt{\frac{\sum_{i=1}^{n} (X_i - M)^2}{n}}$.

Output active power waveform diagram of the VSG-based ADRC strategy and the VSG control strategy are showed in Figure 12. Compared with the VSG control strategy, the output active power fluctuation under the VSG-based ADRC strategy is smaller. Under the VSG control strategy, the RMSE of the output active power is 386.0345, under the VSG-based ADRC strategy, the RMSE of the output active power is 220.0647, Compared to the VSG control strategy, the RMSE is reduced by 43.0%.
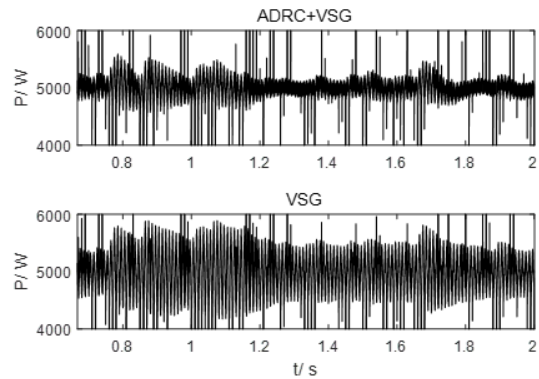

FIGURE 12. Comparison of output active power of two control strategies under big disturbance.
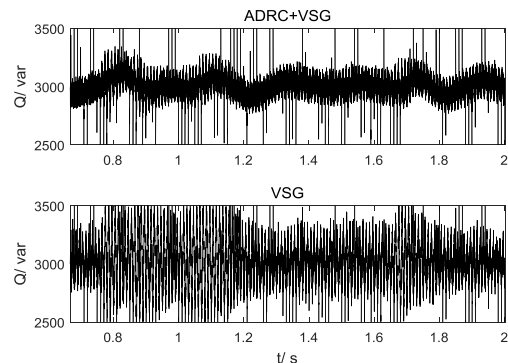

FIGURE 13. Comparison of output reactive power of two control strategies under big disturbance.

Output reactive power waveform diagram of the VSG-based ADRC strategy and the VSG control strategy are showed in Figure 13. Compared with the VSG control strategy, the fluctuation of the output reactive power under the VSG-based ADRC strategy is smaller. Under the VSG control strategy, the RMSE of the output reactive power is 243.1219, under the VSG-based ADRC strategy, the RMSE of the output reactive power is 121.7092, compared to the VSG control strategy, the RMSE is reduced by 49.9%.

Change the intensity of the disturbance, change the noise power of white noise to 0.05W, and the sampling time is 0.01s. The output active power waveform of the VSG-based ADRC strategy and the VSG control strategy are showed

in Figure 14, under the VSG control strategy, the RMSE of the output active power is 226.9230, under the VSG-based ADRC strategy, the RMSE of the output active power is 143.0430, compared to the VSG control strategy, the RMSE is reduced by 37.0%.
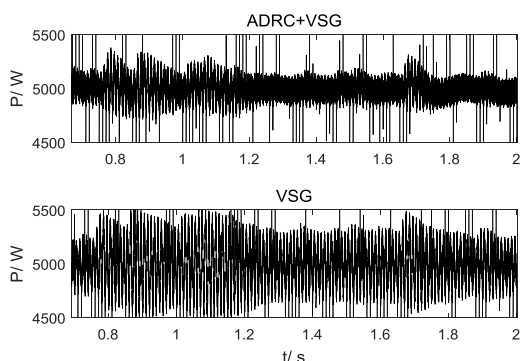

FIGURE 14. Comparison of output active power of two control strategies under small disturbance.
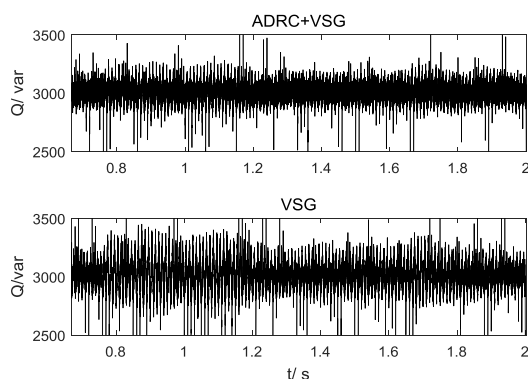

FIGURE 15. Comparison of output reactive power of two control strategies under small disturbance.

The output reactive power waveform of the VSG-based ADRC strategy and the VSG control strategy are showed in Figure 15, under the VSG control strategy, the RMSE of the output reactive power is 138.9878, under the VSG-based ADRC strategy, the RMSE of the output reactive power is 79.6473, compared to the VSG control strategy, the RMSE is reduced by 42.7%. It can be seen from the figure that the VSG-based ADRC strategy can suppress the disturbance well under the disturbance of different intensities.

V. CONCLUSION

This paper proposes ADRC strategy for three-phase unbalanced grid-connected photovoltaic inverter based on VSG. In this paper, the total disturbance is estimated and compensated in advance using ADRC to obtain a new power command value. By the VSG control module, the positive and negative sequence current commands of the inverter output are calculated, Finally, it achieved the control goal of power fluctuations attenuation and improving system dynamic response. The VSG-based ADRC strategy proposed retains the control characteristics of the VSG. It can provide

virtual inertia for the power grid which does not rely on the model and parameters of the controlled system, the system is stable and is not easily affected by external disturbances.

Compared with the traditional VSG control, the control strategy proposed in this paper adds an ADRC link. Through constant adjustment, the appropriate ADRC parameters are selected to improve the ability to suppress disturbance and response speed of the entire system. In contrast, the suppression of the disturbance is more pronounced than improve of response speed, the primary function of the ADRC is to suppress the disturbance. Under the premise of the system output observable, the unknown disturbance is accurately and quickly observed, then the disturbance is compensated, and finally the disturbance of the inverter output power is greatly reduced. The design of the ADRC focuses on the order of the ADRC and the arrangement of the ADRC module, which make the ADRC strategy can be combined with the VSG control strategy, keep the characteristics of the VSG and ensure suppressing disturbance.

The simulation and experimental results show that the addition of the ADRC module makes the VSG-based ADRC strategy has ability to suppress disturbance, which is compared with the VSG control strategy, the disturbance is greatly suppressed and the response speed is also improved.

REFERENCES

[1] T. Shintai, Y. Miura, and T. Ise, "Oscillation damping of a distributed generator using a virtual synchronous generator," *IEEE Trans. Power Del.*, vol. 29, no. 2, pp. 668–676, Apr. 2014.

[2] J. Su, W. Qiu, H. Ma, and P.-Y. Woo, "Calibration-free robotic eye-hand coordination based on an auto disturbance-rejection controller," *IEEE Trans. Robot.*, vol. 20, no. 5, pp. 899–907, Oct. 2004.

[3] J. Liu, Y. Miura, H. Bevrani, and T. Ise, "Enhanced virtual synchronous generator control for parallel inverters in microgrids," *IEEE Trans. Smart Grid*, vol. 8, no. 5, pp. 2268–2277, Sep. 2017.

[4] J. Liu, Y. Miura, and T. Ise, "Comparison of dynamic characteristics between virtual synchronous generator and droop control in inverter-based distributed generators," *IEEE Trans. Power Electron.*, vol. 31, no. 5, pp. 3600–3611, May 2016.

[5] W. Gao and Z.-P. Jiang, "Adaptive dynamic programming and adaptive optimal output regulation of linear systems," *IEEE Trans. Autom. Control*, vol. 61, no. 12, pp. 4164–4169, Dec. 2016.

[6] I. Serban and C. P. Ion, "Microgrid control based on a grid-forming inverter operating as virtual synchronous generator with enhanced dynamic response capability," *Int. J. Elect. Power Energy Syst.*, vol. 89, pp. 94–105, Jul. 2017.

[7] J. Alipoor, Y. Miura, and T. Ise, "Power system stabilization using virtual synchronous generator with alternating moment of inertia," *IEEE J. Emerg. Sel. Topics Power Electron.*, vol. 3, no. 2, pp. 451–458, Jun. 2015.

[8] J. A. Suul, S. D'Arco, and G. Guidi, "Virtual synchronous machine-based control of a single-phase bi-directional battery charger for providing vehicle-to-grid services," *IEEE Trans. Ind. Appl.*, vol. 52, no. 4, pp. 3234–3244, Jul./Aug. 2016.

[9] L.-Y. Lu and C.-C. Chu, "Consensus-based secondary frequency and voltagedroop control of virtual synchronous generators for isolated AC microgrids," *IEEE J. Emerg. Sel. Topics Power Electron.*, vol. 5, no. 3, pp. 443–455, Sep. 2015.

[10] M. A. Torres L, L. A. C. Lopes, L. A. Morán T, and J. R. Espinoza C, "Self-tuning virtual synchronous machine: A control strategy for energy storage systems to support dynamic frequency control," *IEEE Trans. Energy Convers.*, vol. 29, no. 4, pp. 833–840, Dec. 2014.

[11] T. A. Lipo and P. C. Krause, "Stability analysis of a reluctance-synchronous machine," *IEEE Trans. Power App. Syst.*, vol. PAS-86, no. 7, pp. 825–834, Jul. 1967.

[12] Q.-C. Zhong, P.-L. Nguyen, Z. Ma, and W. Sheng, "Self-synchronized synchronverters: Inverters without a dedicated synchronization unit," *IEEE Trans. Power Electron.*, vol. 29, no. 2, pp. 617–630, Feb. 2014.

[13] J. Alipoor, Y. Miura, and T. Ise, "Voltage sag ride-through performance of virtual synchronous generator," in *Proc. Int. Power Electron. Conf.*, May 2014, pp. 3298–3305.

[14] J. Han, "From PID to active disturbance rejection control," *IEEE Trans. Ind. Electron.*, vol. 56, no. 3, pp. 900–906, Mar. 2009.

[15] C. Zhao and Y. Huang, "ADRC based input disturbance rejection for minimum-phase plants with unknown orders and/or uncertain relative degrees," *J. Syst. Sci. Complex.*, vol. 25, no. 4, pp. 625–640, 2012.

[16] S. Li and J. Li, "Output predictor-based active disturbance rejection control for a wind energy conversion system with PMSG," *IEEE Access*, vol. 5, pp. 5205–5214, 2017.

[17] L. A. Castañeda, A. Luviano-Juárez, and I. Chairez, "Robust trajectory tracking of a delta robot through adaptive active disturbance rejection control," *IEEE Trans. Control Syst. Technol.*, vol. 23, no. 4, pp. 1387–1398, Jul. 2015.

[18] Y. X. Su, B. Y. Duan, C. H. Zheng, Y. F. Zhang, G. D. Chen, and J. W. Mi, "Disturbance-rejection high-precision motion control of a Stewart platform," *IEEE Trans. Control Syst. Technol.*, vol. 12, no. 3, pp. 364–374, May 2004.

[19] Q. Zheng, L. Dong, D. H. Lee, and Z. Gao, "Active disturbance rejection control for MEMS gyroscopes," *IEEE Trans. Control Syst. Technol.*, vol. 17, no. 6, pp. 1432–1438, Nov. 2009.

[20] G. Sun, Y. Li, W. Jin, and L. Bu, "A nonlinear three-phase phase-locked loop based on linear active disturbance rejection controller," *IEEE Access*, vol. 5, pp. 21548–21556, 2017.

[21] B.-Z. Guo and F.-F. Jin, "Sliding mode and active disturbance rejection control to stabilization of one-dimensional anti-stable wave equations subject to disturbance in boundary input," *IEEE Trans. Autom. Control*, vol. 58, no. 5, pp. 1269–1274, May 2013.

[22] Z. Wu, G. Huang, C. Wu, C. Lv, and L. Bao, "On convergence of extended state observer for a class of MIMO uncertain stochastic nonlinear systems," *IEEE Access*, vol. 6, pp. 37758–37766, 2018.

[23] Y. X. Su, C. H. Zheng, and B. Y. Duan, "Automatic disturbances rejection controller for precise motion control of permanent-magnet synchronous motors," *IEEE Trans. Ind. Electron.*, vol. 52, no. 3, pp. 814–823, Jun. 2005.

[24] Z.-Q. Gao, "On the foundation of active disturbance rejection control," *Control Theory Appl.*, vol. 30, no. 12, pp. 1498–1510, 2013.

[25] J. F. Pan, N. C. Cheung, and J. M. Yang, "Auto-disturbance rejection controller for novel planar switched reluctance motor," *IEE Proc.-Electr. Power Appl.*, vol. 153, no. 2, pp. 307–316, Mar. 2006.

[26] Q. Chen, L. Li, M. Wang, and L. Pei, "The precise modeling and active disturbance rejection control of voice coil motor in high precision motion control system," *Appl. Math. Model.*, vol. 39, no. 19, pp. 5936–5948, 2015.

[27] M. Guan, W. Pan, J. Zhang, Q. Hao, J. Cheng, and X. Zheng, "Synchronous generator emulation control strategy for voltage source converter (VSC) stations," *IEEE Trans. Power Syst.*, vol. 30, no. 6, pp. 3093–3101, Nov. 2015.

[28] S. D'Arco, J. A. Suul, and O. B. Fosso, "A virtual synchronous machine implementation for distributed control of power converters in smartgrids," *Electr. Power Syst. Res.*, vol. 122, pp. 180–197, May 2015.

[29] H. A. Alsiraji and R. El-Shatshat, "Comprehensive assessment of virtual synchronous machine based voltage source converter controllers," *IET Gener., Transmiss. Distrib.*, vol. 11, no. 7, pp. 1762–1769, Nov. 2014.

[30] G. Wang, B. Wang, C. Li, and D. Xu, "Weight-transducerless control strategy based on active disturbance rejection theory for gearless elevator drives," *IET Electr. Power Appl.*, vol. 11, no. 2, pp. 289–299, Feb. 2017.

[31] H. Wu *et al.*, "Small-signal modeling and parameters design for virtual synchronous generators," *IEEE Trans. Ind. Electron.*, vol. 63, no. 7, pp. 4292–4303, Jul. 2016.

[32] Z.-L. Zhao and B.-Z. Guo, "A nonlinear extended state observer based on fractional power functions," *Automatica*, vol. 81, pp. 286–296, Jul. 2017.

[33] Q. Zhong, Y. Zhang, J. Yang, and J. Wu, "Non-linear auto-disturbance rejection control of parallel active power filters," *IET Control Theory Appl.*, vol. 3, no. 7, pp. 907–916, Jul. 2009.

[34] Y. Ma, W. Cao, L. Yang, F. Wang, and L. M. Tolbert, "Virtual synchronous generator control of full converter wind turbines with short-term energy storage," *IEEE Trans. Ind. Electron.*, vol. 64, no. 11, pp. 8821–8831, Nov. 2017.
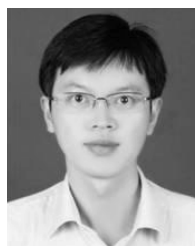
YUNJUN YU was born in Shangrao, China. He received the B.Sc. degree in automation and the M.Sc. degree in control theory and control engineering from Nanchang University, China, in 2000 and 2007, respectively, and the Ph.D. degree from the Chinese Academy of Sciences, in 2013. He is currently an Associate Professor with the Department of Electrical and Automation Engineering, Information Engineering School, Nanchang University. His research interests include fault diagnosis, data-driven optimal control and its application in photovoltaic micro-grid systems, ADRC, and low carbon electricity technology.

XIANGYU HU received the B.Eng. degree from Nanchang University, Jiangxi, China, in 2017, where he is currently pursuing the M.S. degree with the Information Engineering College.

His research interest mainly focuses on inverter.

• • •